Experimental Neurology 372 (2024) 114651

Contents lists available at ScienceDirect

Experimental Neurology

journal homepage: www.elsevier.com/locate/yexnr

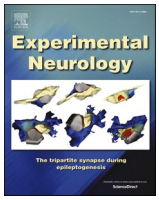

Research paper

Region-specific changes in gene expression are associated with cognitive deficits in the alpha-synuclein-induced model of Parkinson's disease: A transcriptomic profiling study

Maria Francesca Manchinu [a], Mauro Pala [a,1], Maria Francesca Palmas [b,1], Maria Antonietta Diana [a], Andrea Maschio [a], Michela Etzi [b], Augusta Pisanu [c], Francesca Isabella Diana [b], Jacopo Marongiu [b], Silvia Mansueto [d], Ezio Carboni [b], Giuliana Fusco [e], Alfonso De Simone [d], Anna R. Carta [b,*]

[a] National Research Council, Biomedical and Genetic Research Institute, 09040 Cagliari, Italy
[b] Department of Biomedical Sciences, University of Cagliari, 09040 Cagliari, Italy
[c] National Research Council, Institute of Neuroscience, 09040 Cagliari, Italy
[d] Department of Pharmacy, University of Naples "Federico II", 80131 Naples, Italy
[e] Centre for Misfolding Diseases, Department of Chemistry, University of Cambridge, Cambridge, UK

ARTICLE INFO

Keywords:
Alpha synuclein
Oligomers
RNA-seq
Cortex
hippocampus
Cognition

ABSTRACT

Mild cognitive impairment (MCI) is a common trait of Parkinson's disease (PD), often associated with early motor deficits, eventually evolving to PD with dementia in later disease stages. The neuropathological substrate of MCI is poorly understood, which weakens the development and administration of proper therapies.

In an α-synuclein (αSyn)-based model of PD featuring early motor and cognitive impairments, we investigated the transcriptome profile of brain regions involved in PD with cognitive deficits, via a transcriptomic analysis based on RNA sequencing (RNA-seq) technology.

Rats infused in the substantia nigra with human α-synuclein oligomers (H-SynOs) developed mild cognitive deficits after three months, as measured by the two-trial recognition test in a Y-maze and the novel object recognition test. RNA-seq analysis showed that 17,436 genes were expressed in the anterior cingulate cortex (ACC) and 17,216 genes in the hippocampus (HC). In the ACC, 51 genes were differentially expressed between vehicle and H-αSynOs treated samples, which showed $N = 21$ upregulated and $N = 30$ downregulated genes. In the HC, 104 genes were differentially expressed, the majority of them not overlapping with DEGs in the ACC, with $N = 41$ upregulated and $N = 63$ downregulated in H-αSynOs-treated samples. The Gene Ontology (GO) and the Kyoto Encyclopedia of Gene and Genomes (KEGG) analysis, followed by the protein-protein interaction (PPI) network inspection of DEGs, revealed that in the ACC most enriched terms were related with immune functions, specifically with antigen processing/presentation via the major histocompatibility complex (MHC) class II and phagocytosis via CD68, supporting a role for dysregulated immune responses in early PD cognitive dysfunction. Immunofluorescence analysis confirmed the decreased expression of CD68 within microglial cells. In contrast, the most significantly enriched terms in the HC were mainly involved in mitochondrial homeostasis, potassium voltage-gated channel, cytoskeleton and fiber organisation, suggesting that the gene expression in the neuronal population was mostly affected in this region in early disease stages.

Altogether results show that H-αSynOs trigger a region-specific dysregulation of gene expression in ACC and HC, providing a pathological substrate for MCI associated with early PD.

* Corresponding author.
E-mail address: acarta@unica.it (A.R. Carta).
[1] Authors contributed equally to this study.

https://doi.org/10.1016/j.expneurol.2023.114651
Received 31 July 2023; Received in revised form 29 November 2023; Accepted 9 December 2023
Available online 11 December 2023

1. Introduction

Parkinson's disease (PD) is defined as a movement disorder, featured by the appearance of typical motor symptoms, including resting tremor, bradykinesia, rigidity, and postural instability (Dauer and Przedborski, 2003). Even though motor symptoms remain central in PD diagnosis, non-motor symptomatology has been increasingly recognized to heavily weigh on the whole pathological evolution, enough for reconsidering PD as a complex and systemic pathology (Sauerbier et al., 2017). Among non-motor symptoms, hyposmia, constipation, mood changes, and REM sleep behavior disorder (RBD) occur in the prodromal phase of the disease, often preceding the diagnosis of motor PD. Cognitive disturbances also represent a frequent trait, being up to six times more common in individuals with PD than in the healthy population (Aarsland et al., 2021). Cognitive deficits may appear in early motor disease as a mild cognitive impairment (MCI), eventually evolving to dementia in later disease stages (Aarsland et al., 2021; Severiano E Sousa et al., 2022; Williams-Gray et al., 2009). While the neuropathological mechanism underneath motor impairment has been extensively investigated clinically as well as in preclinical PD models, the underlying mechanisms leading to progressive cognitive impairment in PD remain far more elusive. Yet, the identification of neuropathological features associated with cognitive disturbances in the early motor phase of the disease is pivotal to support early recognition and intervention for this invalidating trait.

Most of the current knowledge on MCI pathology in PD comes from clinical studies. These studies have suggested that, among limbic areas, the cingulate cortex (ACC) and hippocampus (HC) subregions are mostly involved in PD-related cognitive disturbances (Christopher et al., 2015; Ekman et al., 2012; Osaki et al., 2009; Sawamoto et al., 2008). At the molecular level, protein misfolding and deposition in limbic cortical regions (Doorn et al., 2014; Kouli et al., 2020; Kövari et al., 2003; Mattila et al., 2000), together with mitochondrial abnormalities (Gatt et al., 2016), inflammatory changes (Edison et al., 2013; Kouli et al., 2020; Williams-Gray et al., 2016) and genetic factors (Aarsland et al., 2017; Collins and Williams-Gray, 2016) have been all investigated as potential pathological contributors. Interestingly, in advanced PD patients the pathology in limbic areas correlated with the cognitive decline, suggesting that Lewy Bodies (LBs) may predict the development of PD with dementia (PDD) (Doorn et al., 2014; Kouli et al., 2020; Kövari et al., 2003; Mattila et al., 2000). However, neocortical LBs are not detectable in the early motor disease with MCI (Aarsland et al., 2021; Braak et al., 2005; Muslimovic et al., 2005), leaving uncertain whether and how the αSyn toxicity in these areas contributes to the MCI pathology in PD. As regard to neuroinflammation, pathological microglia and astroglia have been described in limbic brain regions by Positron Emission Tomography (PET) studies in PD patients (Edison et al., 2013), although this feature was not investigated in relation to cognitive impairment (Doorn et al., 2014; Imamura et al., 2003; Wilson et al., 2019).

Such a shortage of knowledge is largely related to the limited preclinical investigation of cognitive impairment in PD, due to the poor availability of suitable and validated preclinical models aimed at establishing the neuropathological mechanisms of the disease. In recent years, models based on the intracerebral infusion of pathological forms of αSyn have been developed, which largely model the PD neuropathology (Carta et al., 2020; Gómez-Benito et al., 2020). We have characterised an αSyn-based rat model of PD, obtained by the intranigral infusion of human αSyn oligomers (H-αSynOs), and featuring mild motor and cognitive deficits (Boi et al., 2020; Fusco et al., 2017; Palmas et al., 2022a). In such a model, we reported inflammatory events and molecular/functional alterations in the ACC and in discrete HC subregions, suggesting a role for pathological αSyn in cognitive impairment (Palmas et al., 2022b). In addition, other studies have demonstrated the spreading capacity of αSyn toxic species within the mouse brain across anatomically distant regions, including cognition-related limbic areas (Luk et al., 2012; Sorrentino et al., 2017), although this was never investigated in relation to PD symptoms.

Here, we sought to investigate the pathological mechanisms triggered by the intranigral infusion of H-αsynOs in the ACC and HC of rats displaying MCI. Considering the uncertainty and likely multifactorial etiopathogenesis of cognitive disturbances in PD, we used the transcriptomic analysis based on RNA sequencing (RNA-seq) technology to comprehensively approach the neuropathology in these cognition-related brain regions. In recent years, RNA-seq technology has emerged as an efficient high-throughput tool that produces a comprehensive and precise transcriptome profile, allowing the unbiased simultaneous evaluation of multiple transcripts in a single experimental sample. Previous studies using a similar approach have revealed substantial alterations in the transcriptome of brain tissue from PD patients (Benoit et al., 2020; Cappelletti et al., 2023; Chi et al., 2019; Quan et al., 2021) and animal models of PD (Li et al., 2019; Lyu et al., 2021). Specifically, the transcriptome profiling of the frontal cortex from PD patients reported a stage-dependent dysregulation of several signalling pathways (Cappelletti et al., 2023; Xie et al., 2022). However, to our knowledge, few studies have investigated whether and how αSyn may affect the transcriptome of cognitive-related brain regions in preclinical models of PD.

2. Material and methods

2.1. Animals and stereotaxic surgery

Male Sprague–Dawley rats (275–300 g, Envigo) were housed in groups of three to four in standard conditions of temperature (21 ± 1 °C) and humidity (60%) under a 12 h light/dark cycle (lights on 7:00 A.M) with standard diet and water available ad libitum. All procedures were performed in accordance with the ARRIVE guidelines and with the guidelines and protocols approved by the European Community (2010/63UE L276 20/10/2010). Experimental protocols were approved by the Italian Ministry of Health (authorization N. 766/2020-PR).

At 3 months of age, rats were deeply anesthetized with Fentanyl (0.3 mg/kg) and medetomidine hydrochloride (0.35 mg/kg) and stereotaxically injected according to previous studies ($n = 16$) (Boi et al., 2020; Palmas et al., 2022a). H-αSynOs were prepared as previously described (Boi et al., 2020; Palmas et al., 2022a). 5 μL of H-αSynOs were infused bilaterally into the SNpc ($n = 8$) (coordinates relative to bregma; −5.4 mm anteroposterior; ± 1.9 mm from the midline; −7.2 mm beneath the dura, according to Paxinos and Watson's atlas (Paxinos and Watson, 2006) at the rate of 1 μL/min via a silica microinjector as previously described (Boi et al., 2020; Palmas et al., 2022a). The injector was left in place for an additional 5 min after infusion, and then slowly withdrawn. Control animals (Veh, n = 8) received an equal volume of PBS (Fig. 1A, created with BioRender.com).

2.2. Two-trial recognition test in a Y-maze

The effect of H-αSynOs infusion on spatial recognition memory was assessed three-months post-surgery by means of a two-trial recognition test in a Y-maze, as previously described (Palmas et al., 2022b). The maze used in the experiment was made of three symmetrical arms of equal size, each of them was randomly designated as the "start arm," the "novel arm," and the "other arm." The testing procedure involved placing each rat individually in the "start arm" of the maze and conducting two trials separated by a 1-h interval. During trial 1, the "novel arm" was blocked by a guillotine door, while during trial 2, all three arms of the maze were left open for exploration. Visual cues were placed outside the walls of the maze to facilitate navigation by rats.

During trial 1 (10 min), rats were allowed to explore only the "start" and "other" arms, with access to the "novel" arm being blocked. In trial 2 (5 min), rats were allowed to explore all three arms of the maze. Rat behavior was videotaped and subsequently analysed in order to

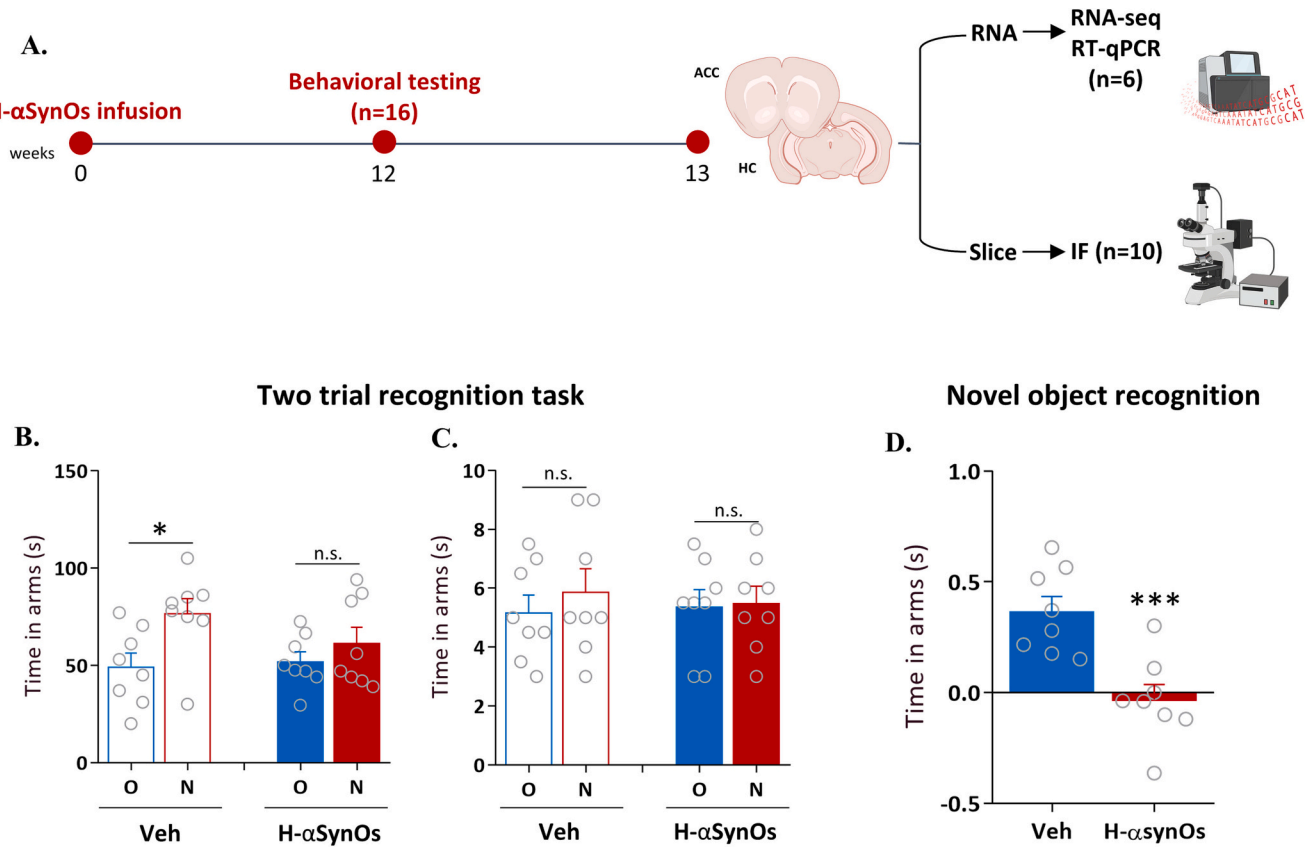

Fig. 1. Schematic illustration of the experimental timeline (A). Time spent in the novel arm (N) and in the other arms (O) in the Two-trial recognition test (B) by vehicle-infused ($n = 8$) and H-αSynOs-infused rats (n = 8) (* $p < 0.05$ by two-way ANOVA followed by Tuckey's post hoc test). Discrimination index measured by the novel object recognition test (C) for vehicle-infused (n = 8) and H-αSynOs-infused rats (n = 8) (*** $p = 0.001$ by Unpaired Student's *t*-test); ACC: anterior cingulate cortex; HC: hippocampus.

determine the number of entries and the time spent in each arm. Spatial recognition memory was evaluated by measuring the preference for the "novel" arm compared to the combination of the "start" and "other" arms, expressed as the number of seconds spent and entries performed in the arms during the second trial (Ferreira et al., 2017).

2.3. Novel object recognition

Novel Object Recognition (NOR) test was carried out in an open field arena (60 × 60 cm) under dim light and according to a previously published protocol (Palmas et al., 2022b). Animals were all tested three-months after H-αSynOs and Veh infusion. The task consisted of three different sessions: habituation, familiarization and testing. During the habituation phase, each rat was placed in the empty arena for 10 min. Thereafter, rats were re-placed individually in the same arena containing two identical objects (10 min - familiarization phase, T1) before returning to their home cages. After a 1-h interval, rats were placed again in the test arena containing one familiar and one novel object (5 min - testing phase, T2). Each phase was videotaped and subsequently analysed. Exploration of an object was defined as directing the nose to the object at a distance <2 cm and/or touching it with the nose. Object recognition was expressed by the discrimination index (DI) according to the following formula: (Tn-Tf)/(Tn + Tf) (Tn = time spent exploring the novel object; Tf = time spent exploring the familiar one). A DI value greater than zero indicated that mice spent more time exploring the novel object, suggesting recognition memory for the familiar object.

2.4. RNA isolation, library preparation and sequencing

Three-months after surgery, rats were deeply anesthetized, and brains were carefully removed from the skull ($n = 3$ from each experimental group). ACC and HC regions from both hemispheres were dissected and pooled immediately afterward in a pre-cooled sterile Petri dish on ice. The brain tissue was immediately transferred to an RNAse-free Eppendorf tube, snap-frozen in liquid nitrogen, and stored at −80 °C until RNA extraction. Total RNA was subsequently extracted using the PureLink® RNA Mini Kit (Ambion #12183018 A) according to the manufacturer's instructions. The quantity and the integrity of isolated RNA samples were evaluated using the Agilent 2100 Bioanalyzer (Agilent Technologies, Palo Alto, CA, USA). RNA-seq libraries were prepared with an Illumina® Stranded mRNA Prep, Ligation Kit (Illumina #20040532) and IDT® for Illumina® RNA UD Indexes Set A, Ligation (Illumina #20040553) according to the manufacturer's instructions.

The RNA library concentration was measured using a Qubit® 2.0 fluorometer and successfully sequenced on an Illumina NovaSeq6000 (Illumina Inc., San Diego, CA, USA).

2.5. RNA-seq data analysis

RNAseq short reads quality has been evaluated with FASTQC (v0.11.9) (Andrews, 2010) software (Supp Table 1), showing good quality for all samples. *Rattus norvegicus* reference genome (primary assembly, mRatBN7.2) was downloaded from ENSEMBL web site (http://ftp.ensembl.org). Short reads were aligned to the reference genome with STAR software (2.7.9a) (Dobin et al., 2013). Genes coordinates (Rattus_norvegicus.mRatBN7.2.105.gtf) were downloaded from ENSEMBL web site (http://ftp.ensembl.org) and gene expression level was evaluated with HTSeq software (Anders et al., 2015) (0.11.3) with the following command line: htseq-count –stranded = reverse –mode = union –idattr = gene_id –type = exon.

Potential latent confounders were visually investigated with Principal Component Analysis (PCA) and inferred with the svaseq software (Leek, 2014). Only genes showing at least 5 reads in the 25% of the samples were analysed for differential expression (between vehicle and H-αSynOs) with the DESeq2 software (Love et al., 2014) by using defaults settings. We performed differential expression both with and without incorporating the svaseq confounders in the DESeq2 model.

In the downstream analysis, we used the model incorporating the svaseq confounders. In both comparisons, in ACC and HC samples, only one Surrogate Variable - SV - was identified by svaseq, thus the model used was "Yg ~ SV_1 + treatment", in which Yg is a vector of gene expression of gene g, SV_1 is the vector of the SV identified with svaseq, and treatment is a vector indicating whether the sample was vehicle or H-αSynOs.

We explored the contribution (correlation) of phenotypical and technical variables to the SVs. We first confirmed that the SVs did not correlate with the treatment vector (in ACC Pearson *p*-value = 0.6, Spearman p-value = 1; in HC Pearson p-value = 0.8, Spearman p-value = 0.75) supporting that the SVs captured unwanted sources of variation while preserving the biological variation of interest (the treatment vector).

We then correlated the SVs with the quality control metrics of the RNAseq measurements (identified by FASTQC software and by STAR software, reported in the "Log.final.out" file).

For the SV identified in ACC samples, we found nominally significant correlation with a STAR metric regarding the number of unmapped reads "too short" (Pearson r^2 = 0.64, p-value = 0.0166) which varied from 0.92 to 2.9 million of reads among the samples. For the SV identified in HC samples, we found nominally significant correlation with a FASTQC metric related to the presence of a "WARNING" for overrepresented sequences (Spearman rho = −0.79, p-value = 0.034; Pearson r2 = 0.60, p-value = 0.042). The overrepresented sequence in question was a poly-N, with abundance ranging from 0.11% to 0.8%.

FDR was computed with the Benjamini-Hochberg method. Because the distribution of *p*-values was far from a uniform distribution, we recomputed p-values with the fdrtools R package (Strimmer, 2008) and the relative FDR with the Benjamini-Hochberg method. We considered DEGs those genes at FDR 5%, without requiring a predefined fold change threshold.

2.6. Gene ontology, KEGG pathway analysis and PPI network of DEGs

Gene Ontology (GO) is an ontology widely used in the field of bioinformatics for annotating large scale genes and gene products (Harris et al., 2004). It covers 3 aspects of biology: biological process (BP), molecular function (MF), and cellular component (CC). The Kyoto Encyclopedia of Genes and Genomes (KEGG) is a practical database resource for genome sequencing and polymer experiment technology. It is generated by molecular level information, especially macromolecular datasets, which can be used to predict pathways in which a particular gene is enriched (Kanehisa et al., 2017). GO analysis and KEGG analysis were performed by g:Profiler toolset (Raudvere et al., 2019) (https://biit.cs.ut.ee/gprofiler), used to analyse the enrichment of DEGs in the database of GO and KEGG. Plots were generated with custom R scripts. The Venn tool (http://bioinformatics.psb.ugent.be/webtools/Venn/) was used to compose Venn diagrams for DEGs.

Protein-protein interaction (PPI) analysis of DEGs was based on a STRING database (Szklarczyk et al., 2015) and Cytoscape software.

2.7. Reverse transcription-quantitative PCR (RT-qPCR)

Total RNA was extracted using PureLink® RNA Mini Kit as described above. The cDNA was synthetized using random primers and a reverse transcription kit SuperScript™ III First-Strand Synthesis System (Cat# 18080–051, Invitrogen) according to the manufacturer's procedure. RT-qPCR was performed using Platinum SYBR® Green (Cat # 11744–100 Invitrogen) on ABI PRISM 7900 thermocycler (Applied Biosystems, Foster City, CA, USA).

The following primers were used:

RT1-Db1: Fw 5′AGAGTCGAGTGGAAAGCACA 3'-Rev 5′GAAGAGCAGACCCAGACGAT 3′.

RT1-Da: Fw 5′GGTCAATGTCACCTGGCTTC 3′-Rev 5′ GGAATTTGCGGAAGAGGTGG 3′.

CD74: Fw 5′AGGCCACCACTGCTTACTTC 3′-Rev 5′CAGGTTTGGCAGATTTCGGA 3′.

RT1-Ba: Fw 5′ ATCCAGAGGCCAGTACACAC 3′-Rev 5′ GTCAGTTGTCCAAACTCGGG 3′.

CD68: Fw 5′AACAAAACCAAGGTCCAGGG 3′-Rev 5′TACTGTGGCTCTGATGTCGG 3′.

Gapdh: Fw 5′GGCTGCCTTCTCTTGTGACA 3′-Rev 5′ TGAACTTGCCGTGGGTAGAG 3′.

b-Actin: Fw 5′TCAACACCCCAGCCATGTAC 3′-Rev 5′ TCCGGAGTCCATCACAATGC 3′.

The target gene expression level was normalised to *Gapdh* and *b-Actin* mRNA expression levels. RT-qPCR was performed in triplicate and the analysis data was done using the DDCT method.

2.8. Immunohistochemistry

At the end of the behavioral testing, rats were anesthetized and transcardially perfused in ice-cold 0.1 M PBS (pH 7.4) followed by 4% formaldehyde (n = 5 from each experimental group). Thereafter, brains were post-fixed overnight in the same fixative and stored in 0.1% NaN3-PBS at 4 °C. Free-floating coronal brain sections of 40 μm thickness were vibratome-cut at the level of the ACC (Bregma: +2.16 to +0.36).

For immunofluorescence analysis, ACC sections were pre-incubated in BSA/normal donkey serum blocking solution and then immunoreacted with the following unconjugated primary antibodies: goat polyclonal anti Iba-1 (1:1000, Novus Biologicals), mouse monoclonal anti CD68 (1:100, BioRad), rabbit polyclonal anti TGF-β (1:200, Abbiotec) and rabbit polyclonal anti EEAT2/GLT-1 (glutamate transporter type 1, 1:200, Synaptic Systems). For fluorescence visualization of Iba-1 a two-step indirect labelling protocol was used, while a three-step detection was performed to increase the signal of CD68, TGF-β and GLT-1 by combining biotin SP-conjugated IgG (1:200, Jackson Immunoresearch) and streptavidin–fluorescein (1:400, Jackson Immunoresearch). Sections were thereafter counterstained with DAPI (1:1000).

2.9. Confocal microscopy analysis

A spinning disk confocal microscope (Crisel Instruments, Rome, Italy) was used for qualitative and quantitative analyses of Iba-1, CD68, TGF-β at 63× magnification. For the colocalization analysis of CD68 within Iba-1+ cells, a stack from each dataset (40 images) was first obtained. Thereafter, in the resulting stacks, 10 regions of interest for the ACC (x = 700 μm; y = 700 μm; z = 40 μm) in each acquired section and for each animal were randomly chosen, and the volume of the elements calculated. Specifically, three-dimensional isosurfaces were created with the Surfaces module from both Iba-1 and CD68 channels. A new channel was then generated from the colocalization, and a 3D isosurface of overlapping areas was created.

For quantification of staining intensity of GLT-1, total cell and background staining were measured using ImageJ software (NIH), and the intensity of specific staining was calculated.

3. Results

3.1. H-αSynOs-induced cognitive deficits

Confirming previous studies, the intranigral infusion of H-αSynOs induced a MCI within the memory domain that was significant three months post-infusion (Palmas et al., 2022b) (Fig. 1B). Short-term

memory was assessed by means of two different cognitive tasks: the two-trial recognition test in a Y-maze and the NOR. Three months post-intranigral infusion of H-αSynOs, rats developed a mild but significant deficit in the spatial recognition memory, as revealed by a reduced preference for the novel arm during the T2 in the two-trial recognition task. Two-way ANOVA followed by Tuckey post-hoc test showed a distinct preference for the novel arm by vehicle-infused animals, expressed as the total time spent in the novel vs the other two arms (expressed as the mean value between the time spent in the 'entry' arm and in the 'other' arm; * $p < 0.05$ by two-way ANOVA followed by Tuckey's post hoc test). By contrast, H-αSynOs-infused animals spent a similar amount of time in the different arms (Two-way ANOVA, followed by Tuckey' post-hoc test; $p = 0.9217$). No changes were observed in the number of entries between arms (Fig. 1C), indicating that the spatial memory impairment was not related to motor deficits.

Such an impairment to recognize novelty was also observed in the NOR test (Fig. 1C). Specifically, H-αSynOs-infused rats were unable to discriminate between objects and the unpaired Student's *t*-test showed a significant difference when comparing the DI of vehicle vs. H-αSynOs-infused rats ($t = 4154$; $p < 0.0010$), suggesting a deterioration in recognition memory of H-αSynOs-infused animals.

3.2. The H-αSynOs induced region-specific changes in gene expression in ACC and HC

In rats infused within the substantia nigra with H-αSynOs and displaying MCI, we performed the RNA-seq to characterise the transcriptomic profile of the ACC and HC (Fig. 2).

757,859,290 paired-end reads were obtained altogether in the library, which corresponds to an average of 47,366,205.6 paired-end reads per sample. We found that 17,436 genes were expressed in ACC and 17,216 genes in HC.

ACC: differential gene expression analysis identified 51 genes that were differentially expressed in the ACC between untreated and treated samples. Of these genes, $N = 21$ were upregulated and $N = 30$ were downregulated in treated samples (P-value <0.05 compared with the untreated group (Fig. 2A and D).

HC: in the HC, we found 104 genes differentially expressed. $N = 41$ were upregulated and $N = 63$ were downregulated in treated samples (P-value <0.05 compared with the untreated group, (Fig. 2 B and E). All the DEGs, upregulated and downregulated in the two brain regions are also presented in Supp. Table 1 and 2.

We further analysed the overlapped DEGs between the two brain regions and only found 7 overlapping DEGs, namely *Vps52*, *RT1-16CE*, *Csrp1*, *Cryab*, *Slc7a5*, *Abcg2* and *NA* (Fig. 2C), suggesting that H-αSynOs produced a largely different effect on the transcriptome profile of the two brain regions.

3.3. GO and KEGG pathway analyses show different DEGs-functional clusters in ACC and HC

Bioinformatics analysis using the Gene Ontology (GO) and the Kyoto Encyclopedia of Gene and Genomes (KEGG) databases was applied to interpret the related function of the differentially expressed genes. The DEGs were classified into the three main categories: biological process (BP), cellular component (CC) and molecular function (MF), after sorting by P-value.

ACC. In the ACC several significantly enriched terms were found in BP, CC and MF classes. Interestingly, in this brain region most terms were related with immune functions, specifically with antigen processing/presentation via the major histocompatibility complex (MHC) class II (Fig. 3A).

HC. Unlike the ACC, the most significantly enriched BP terms in the HC were mainly involved in anatomical structure development and morphogenesis, neurogenesis and in fiber organisation, suggesting that the neuronal population was mostly affected in this region. No significantly enriched MF terms were obtained in HC (Fig. 3B).

To explore the dysregulation at the level of signalling pathways, we compared the KEGG pathways between the H-αSynOs-infused and vehicle-infused rats. The KEGG pathway analysis is used to predict the biological processes and phenotypic traits of genes. To analyse the functional alterations in signalling pathways induced by H-αSynOs, the DEGs of the ACC and HC were mapped versus a reference canonical signalling pathway, via KEGG database analysis. According to a P value < 0.05 as the standard, the DEGs in ACC were significantly enriched in 14 pathways, with the most significant pathways being "Antigen processing and presentation" (Fig. 4). In contrast, not statistically enriched KEGG pathway in HC was found.

Interestingly, the GO and KEGG analysis revealed several significantly enriched terms in the ACC, most of them being related with immune functions involved in antigen processing/presentation via the MHC-II complex (encoded in humans by the *HLA-DR* genes) and in phagocytosis, supporting a role for dysregulated immune responses in PD cognitive dysfunction.

In particular, the GO:CC analysis showed a downregulation of the MHC-II related genes *Cd74*, *RT1-Db1*, *RT1-Da* and *RT1-Ba*. The RT-qPCR performed to validate these results confirmed the downregulated gene expression in the ACC of H-αSynOs-infused rats (Fig. 5).

3.4. PPI analysis of DEGs in the ACC and HC

We sought to get more insight into the genes differentially expressed in ACC and HC by further exploring them by PPI networks. One network for each tissue (ACC and HC) was constructed (Fig. 6A and B) with the input of 51 DEGs in ACC and 104 DEGs in HC respectively. In the ACC the computed network comprised 14 nodes, 3 of which, corresponding to genes *SMAD3*, *CD68* and *SLC1A2*, had the highest node degree. Specifically, *SMAD3* resulted upregulated (log2FC = 0.28, *p*-value 1.12E-05), *CD68* was downregulated (log2FC = −0.99, p-value = 4.53E-05) and *SLC1A2* was upregulated (log2FC = 0.27, $p = 2{,}42E\text{-}07$).

In the HC the computed network comprised 41 nodes, 3 of which, corresponding to genes *KCNA1*, *CRYAB* and *VIM*, had the highest node degree. Specifically, *KCNA1* (log2FC = −0.15, p-value = 4.41E-07), *CRYAB* (log2FC = −0.27, p-value = 5.13E-05) and *VIM* (log2FC = −0,3, p-value = 5.86E-06) were all found downregulated.

3.5. Key proteins expression in the ACC

Since the PPI analysis revealed that the phagocytic marker CD68 owned the highest node degree within the network, the mRNA and protein levels were further analysed and measured by RT-qPCR and IF to identify the sourcing cell population in the ACC of H-αSynOs and Veh-infused rats. Fig. 7A shows that *CD68* mRNA expression was downregulated when measured by RT-qPCR. The IF colocalization analysis revealed that protein levels were downregulated within microglial cells in the ACC of rats infused with H-αSynOs as compared to Veh-infused rats ($p < 0.001$ by Mann-Whitney non-parametric test). We also analysed the protein levels of GLT-1 (encoded by gene SLC1A2) and confirmed the upregulation of this transporter in the ACC of H-αSynOs-infused rats ($p < 0.01$ by Unpaired Student's *t*-test).

Moreover, since *SMAD3* is a main effector of the canonical signalling of transforming growth factor (TGF)-β, and because TGF-β is highly involved in PD and αSyn-oligomers toxicity (Diniz et al., 2020), we analysed its expression via IF (Fig. 8). As shown in Fig. 8A-B, TGF-β labelling was highly increased in ACC of H-αSynOs-infused rats as compared to vehicle-infused rats ($p < 0.0001$ by Mann-Whitney non-parametric test).

4. Discussion

The present study was aimed at identifying transcriptional modifications occurring in cognition-related brain regions in a

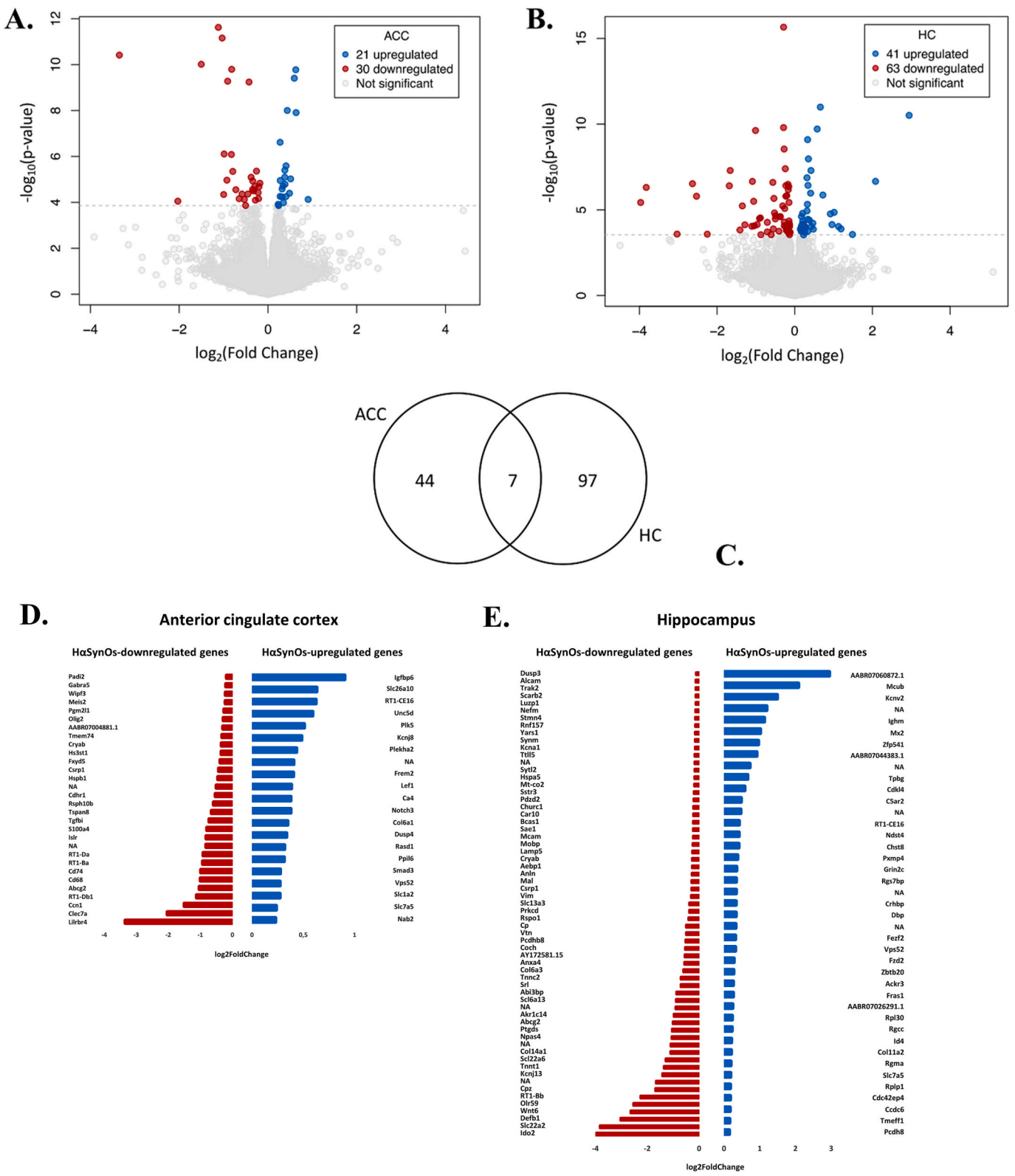

Fig. 2. Identification of the DEGs in the ACC and HC from H-αSynOs-infused ($n = 3$) and vehicle-infused (n = 3) rats. (A-B) Volcano plots of the DEGs in the ACC and HC. The x-axis represents the |log2foldchange| of the DEGs. The y-axis represents the statistical significance of the DEGs (padj). Blu dots represent the upregulated DEGs, red dots represent the downregulated DEGs, and gray dots represent genes with no significant differences. (C) Venn analysis of the DEGs in the two brain regions. (D-E) Differentially expressed genes in ACC and HC. (For interpretation of the references to colour in this figure legend, the reader is referred to the web version of this article.)

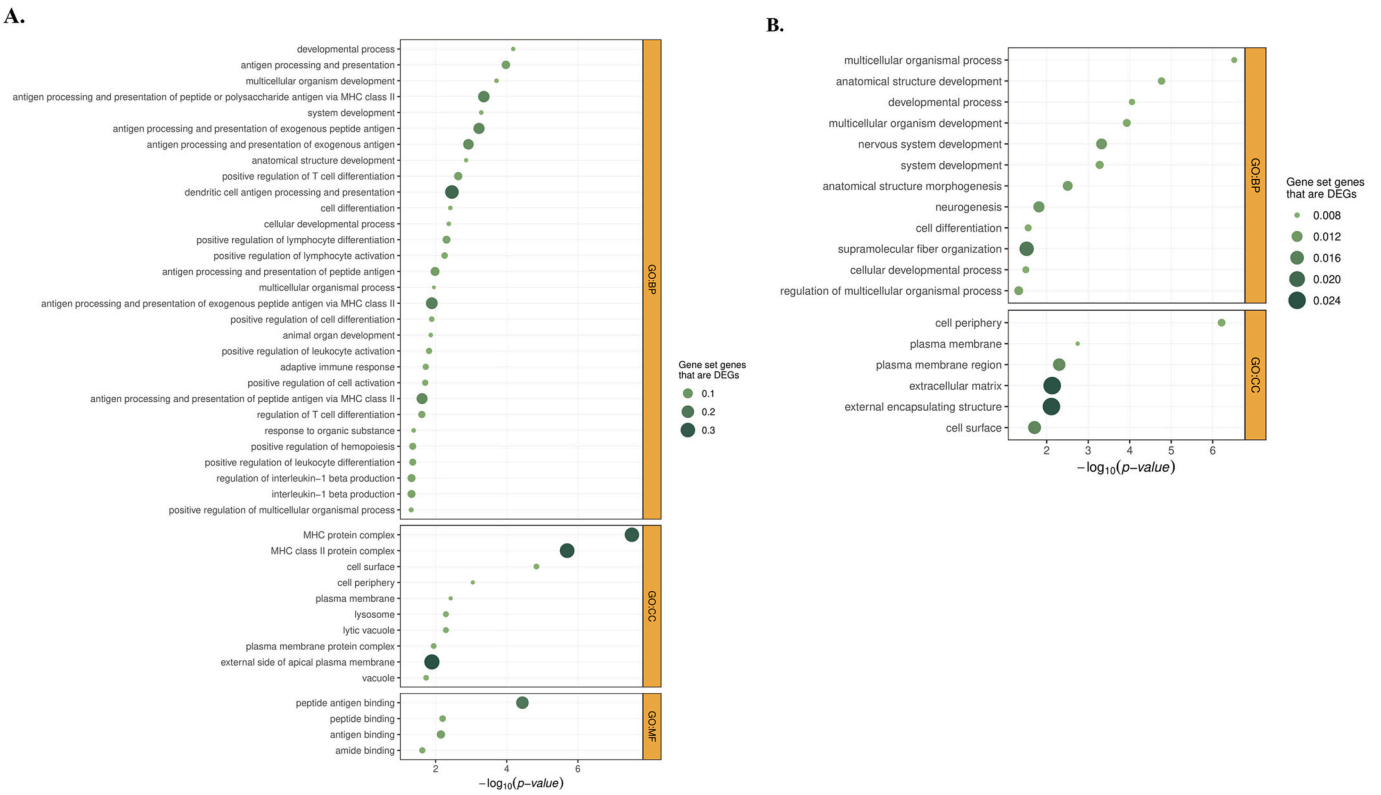

Fig. 3. GO analysis performed with gProfiler on the DEGs in ACC (A) and HC (B) from H-αSynOs-infused rats (n = 3) and vehicle-infused rats (n = 3). The size of the plots indicates the proportion of the number of genes in the GO term that were differentially expressed (DEGs).

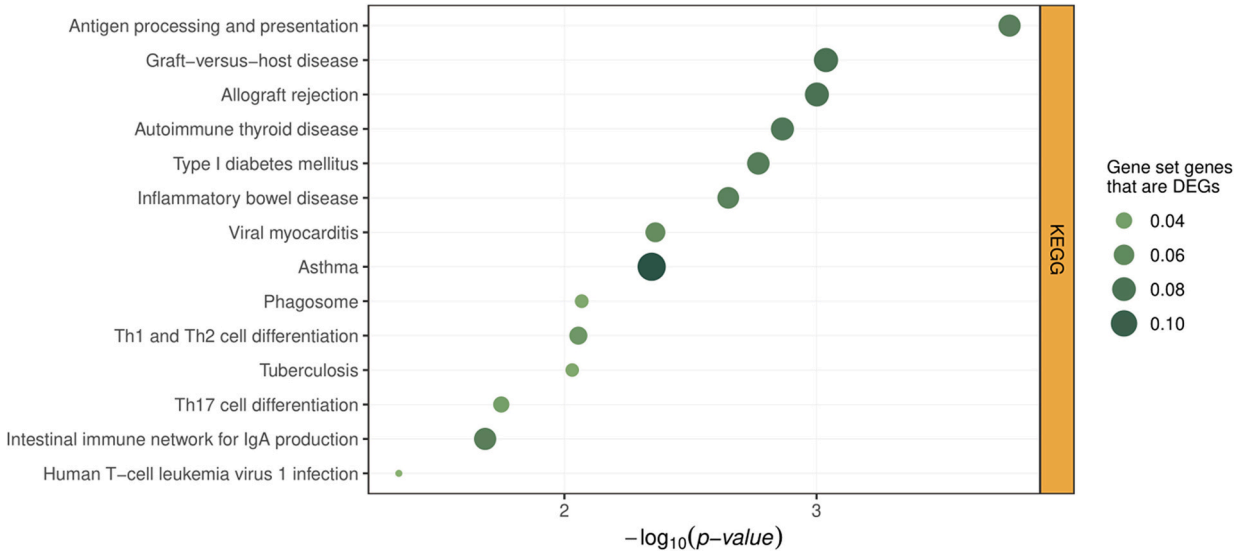

Fig. 4. KEGG pathway analysis performed with gProfiler on the DEGs in ACC from H-αSynOs-infused rats (n = 3) and vehicle-infused rats (n = 3). The size of the plots indicates the proportion of the number of genes in the GO term that were differentially expressed (DEGs).

neuropathological model of early PD based on the intranigral infusion of H-αSynOs. That PD model has been previously characterised to feature several symptomatic and histological hallmarks of early motor PD. Three months after H-αSynOs infusion, rats display symptoms including mild motor impairment underlain by a partial nigrostriatal degeneration and phospho-αSyn deposits, concurrent MCI and neuroinflammation in both motor and cognitive brain regions, altered electrophysiological parameters in cognitive regions (Boi et al., 2020; Palmas et al., 2022b).

As a main finding of the present study, the infusion of H-αSynOs within the SN triggered region-specific changes in the transcriptome profile of distant regions such as the ACC and the HC, while inducing MCI as shown previously. Among 17,436 genes expressed in the ACC and 17,216 in the HC, respectively 51 and 104 were differentially expressed in the PD condition, with roughly 40% being upregulated and 60% downregulated. Of note, only 7 DEGs overlapped between the two regions, indicating that changes in gene expression induced by the H-αSynOs were region-specific. Accordingly, the affected gene patterns were referable to different functional clusters, as shown by the KEGG

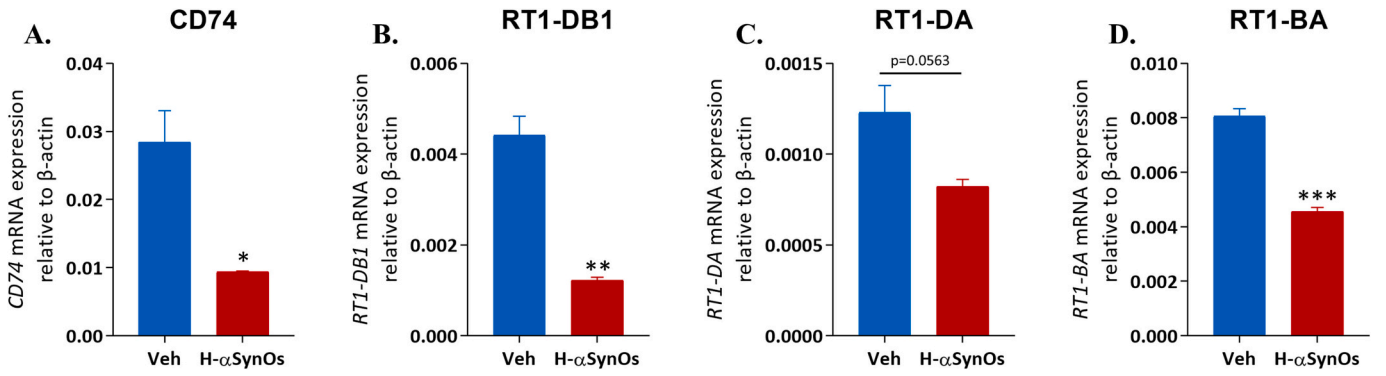

Fig. 5. Cd74, RT1-Db1, RT1-Da, RT1-Ba mRNA expression measured by RT-qPCR and normalised to the housekeeping gene Beta-actin (*p < 0.05, **p < 0.01, ***p < 0.001 by Unpaired Student's t-test; n = 3 animals per group).

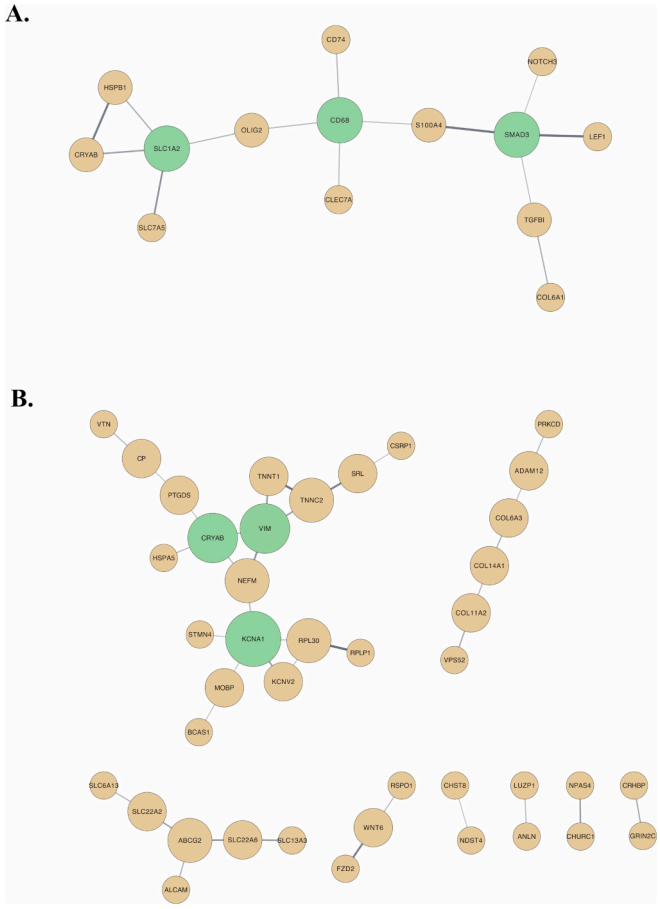

Fig. 6. PPI network constructed with DEGs identified in ACC (A) and HC (B). Only genes with at least one edge with other genes were shown.

pathway analysis used to predict the biological processes and phenotypic traits of genes. The KEGG analysis showed that the DEGs in ACC were significantly enriched in 14 pathways, with the most significant being "Antigen processing and presentation". In contrast, genes involved in neuronal functions were mainly affected in the HC, while there was not statistically enriched KEGG pathway in this region.

The results demonstrate αSyn-dependent changes in cognitive related regions, strongly suggesting a neuropathological role of αSyn toxic species in MCI associated with early motor PD. Of note, we did not detect any deposit of aggregated αSyn in the analysed cortical regions (data not shown). In a previous study, we found that the same protocol of H-αSynOs infusion induced both neuroinflammation and changes in neuronal firing rate in these regions, without detectable protein aggregates (Palmas et al., 2022b). Accordingly, in early motor PD patients with MCI, αSyn deposits were not detectable in limbic regions (Aarsland et al., 2021; Braak et al., 2005; Muslimovic et al., 2005). Moreover, a recent RNAseq study in the frontal cortex from PD patients at different Braak stages, reported an altered gene expression in early stages preceding clear LBs deposition (Cappelletti et al., 2023). αSynOs are small soluble species, not detectable histologically, which may reach distant cortical areas by a spreading process through the connectome (Luk et al., 2012; Sorrentino et al., 2017).

The H-αSynOs triggered a dysregulation of immune functions in the ACC. The DEGs analysis and the following GO and KEGG, and PPI analysis revealed that several significantly enriched terms were found in the ACC, most of them being related with immune functions involved in antigen processing/presentation via the MHC-II complex (encoded in humans by the HLA-DR genes) and in phagocytosis, supporting a role for dysregulated immune responses in early PD cognitive dysfunction. Specifically, we found that the expression of at least 4 components of the MHC-II protein complex, namely *RT1-Db1*, *RT1-Da*, *Cd74* and *RT1-Ba* and the phagocytic marker *CD68* were downregulated in the ACC three months post-infusion of H-αSynOs. The PPI analysis confirmed a critical role of *CD68*, which displayed the highest node degree in connection with the MHC-II gene *Cd74*.

The MHC-II complex enables antigen presentation by antigen presenting cells (APCs) to CD4+ T lymphocytes for adaptive immune responses, and in the brain is mainly expressed by microglia. It shuttles to the lysosomal compartment within the cell, to be loaded with lysosome-processed antigen for presentation at the plasma membrane (Dani et al., 2004). CD68 is a lysosomal glycoprotein involved in the phagocytic machinery, classically considered a marker of phagocytic microglia. Accordingly, IF colocalization experiments performed in our study showed an intracytoplasmic CD68 pattern in microglia of vehicle-infused rats, consistent with the labelling of lysosomes, which was almost absent in the ACC of H-αSynO-infused rats. Therefore, results clearly demonstrate that H-αSynOs induce the dysfunction of a pivotal clearing mechanism engaged by microglia to protect neurons from dangerous signals, as it is the MHC-II/phagocytosis/lysosome machinery. The pathological role of dysfunctional lysosomal pathways was previously demonstrated in fibroblasts obtained from PD patients bearing a *GBA* mutation (García-Sanz et al., 2017, 2018). Moreover, previous studies have shown a proinflammatory microglia profile in the ACC of H-αSynOs-infused rats (Palmas et al., 2022b). Altogether, the data indicate that a gain of inflammatory function and a loss of APC function by microglia in the ACC is a neuropathological substrate of MCI in our PD model. In line with our study interestingly, studies investigating the role of MHC-II and microglial phagocytosis in PD have suggested that their expression in motor-related brain regions is dependent on the disease stage (Boi et al., 2020; Dijkstra et al., 2015; Durrenberger et al., 2015; Harms et al., 2013; Lecca et al., 2018; Pisanu et al., 2014;

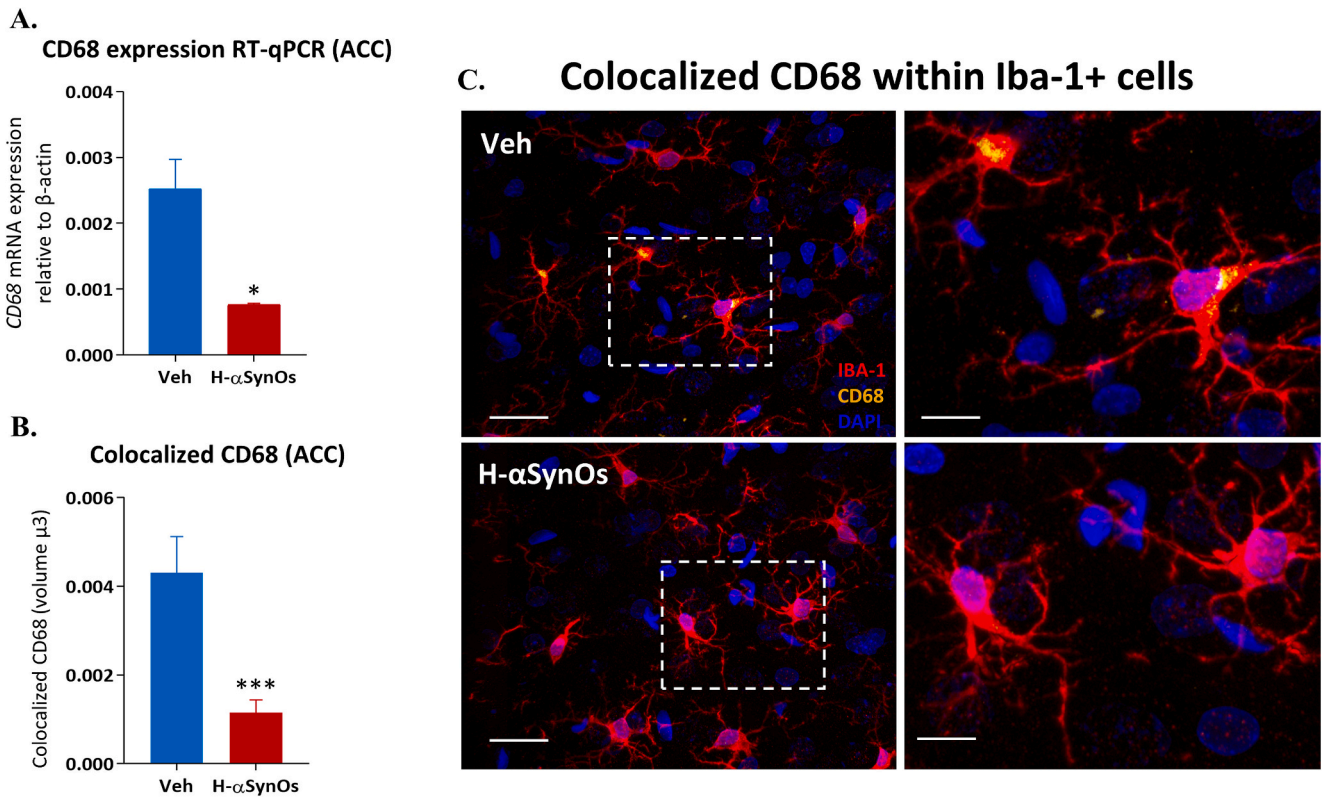

Fig. 7. CD68 levels in the ACC of HαSynOs- and Veh-infused rats. (A) CD68 mRNA expression levels measured by RT-qPCR, normalised to the housekeeping gene β-actin (*p < 0.05, by Unpaired Student's t-test; $n = 5$ animals per group).
(B) Representative images of CD68 (yellow) colocalized with Iba-1+ cells (red). Magnification 63×; scale bars: 20 µm (left); 5 µm (right). (C) Volume of colocalized CD68 within microglial cells in the ACC. (***p < 0.001 by Mann-Whitney non-parametric test; n = 5 animals per group). (For interpretation of the references to colour in this figure legend, the reader is referred to the web version of this article.)

Rostami et al., 2020), showing an upregulation in early PD, but not in later stages of the disease. Moreover, microglial cells exposed in vitro to H-αSynOs gradually lose their phagocytic capacity (Boi et al., 2020). Importantly, a recent study performing the transcriptome analysis of frontal cortical areas from PD patients clearly showed disease stage-specific changes of genes involved in immune responses (Cappelletti et al., 2023). In line with our results and adding translational value to our model, pathways involved in the innate response, included inflammatory cytokine production, were upregulated early in the disease, while genes involved in adaptive immune responses such as antigen presentation and in phagocytosis were found downregulated in later neuropathological stages (Cappelletti et al., 2023). In addition, the gene wide association (GWAS) analysis revealed 5 genes differentially expressed at late PD stages and located near to a PD risk single nucleotide polymorphism, among which *SCARB2*, encoding for a scavenger receptor gene, was differentially expressed in our model (Cappelletti et al., 2023). Therefore, both innate and adaptive functions are dysregulated by αSynOs; in the early disease pathogenesis microglia may be immunologically reactive to cope with the danger, while they lose such a defensive function in later stages maintaining the inflammatory profile.

Supporting a role of αSyn-induced immune responses in cognitive deficits, αSyn pathology was shown in the ACC of PDD patients and correlated with microglia activation and T-cell infiltration (Kouli et al., 2020). Moreover, human imaging studies have shown an inflammatory environment in limbic areas of patients affected by PDD (Edison et al., 2013; Fan et al., 2015). Our results extend the accumulating reports of αSyn-induced immune responses in motor-related areas in PD: aggregated αSyn accumulates on microglia and is taken up into the autophagosome compartment (Boi et al., 2020; Cao et al., 2012); CD4+ T cells from PD patients specifically react to αSyn-specific MHC-II epitopes (Lindestam Arlehamn et al., 2020; Sulzer et al., 2017); infiltrates of T cells have been described in the mesencephalic tissue of PD patients and of H-αSynO-infused rats (Brochard et al., 2009; Jung et al., 2021).

The PPI analysis indicated that *SMAD3* and *SLC1A2* (encoding for GLT-1), were the other two network nodes with the highest degree of connections. Both *SMAD3* and *SLC1A2* gene expression were upregulated by H-αSynOs infusion in the ACC. *SMAD3* is a main effector in the canonical signalling of transforming growth factor (TGF)-β (Massagué and Wotton, 2000). The *GLT-1* is the main glutamate transporter on astrocytes, on which it is exclusively expressed, and its levels are dynamically regulated by neuroglial interactions and growth factors such as the *TGF-β* (Koeglsperger et al., 2013). Of note, we found that *TGF-β* was also overexpressed in the ACC of cognitively impaired rats. Together with previous evidence of αSynO-induced astrocytosis in this area, results suggest an astrocytic response in the ACC, involving a TGF-β-mediated mechanism likely triggering the *GLT-1* upregulation (Palmas et al., 2022b). Previous studies have shown that αSyn oligomers increased astrocytic *GLT-1* levels via a TGF-β-mediated mechanism both in vitro and in vivo in motor brain regions (Diniz et al., 2020). Moreover, a dysfunctional astrocyte-controlled glutamate homeostasis impacted on cognition in senescence and in neurodegenerative diseases (Todd and Hardingham, 2020), and it was recently reported that astrocytic *GLT-1* was upregulated in cognitive brain regions of aged mice (Matias et al., 2023). Interestingly, besides the many genes involved in the immune response, genes with a role in cellular activity were downregulated in the ACC, including the *GABRA5* subunit of GABA receptor, which regulation depends on the TGF-β/SMAD3 pathway. This finding is in line with our previous report of suppressed firing frequency of pyramidal cells in the ACC following H-αSynOs infusion (Palmas et al., 2022b).

H-αSynOs triggered a dysregulation of neuronal homeostasis molecules in the HC. The intranigral infusion of H-αSynOs induced several changes in gene expression in the HC, affecting different functional

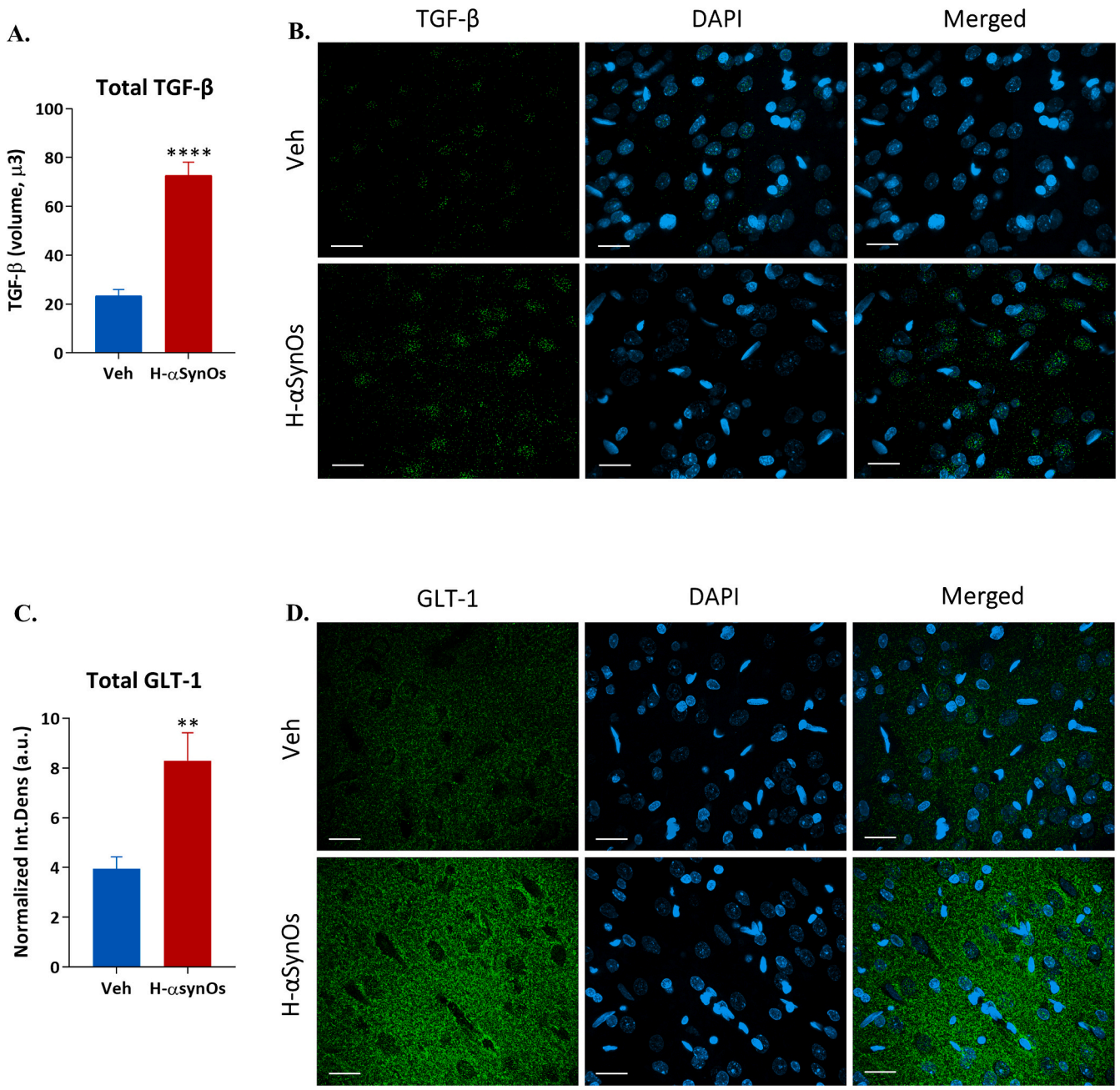

Fig. 8. TGF-β and GLT1 levels in the ACC of HαSynOs- and Veh-infused rats. (A) Volume of total TGF-β analysed in discrete regions of the ACC. (B) Representative images of TGF-β (green) in the ACC of Veh (up) and HαSynOs-infused (down) rats. (C) Immunoreactivity of total GLT-1. (D) Representative immunofluorescence images of GLT-1 (green) in the ACC of Veh (up) and HαSynOs-infused (down) rats. Magnification 63×; scale bars: 20 µm. (****$p < 0.0001$ by Mann-Whitney non-parametric test, **$p < 0.01$ by Unpaired Student's t-test; $n = 5$ animals per group). (For interpretation of the references to colour in this figure legend, the reader is referred to the web version of this article.)

clusters than DEGs identified in the ACC. Of note, among the 7 overlapping DEGs between the two regions, none was involved in immune responses, suggesting different H-αSynOs-triggered mechanisms. The most upregulated genes in the HC were connected with mitochondrial homeostasis, cytoskeleton, neurodevelopment and neurogenesis. Of note, the *Mcub* gene was highly upregulated in HC of H-αSynOs-infused rats. *Mcub* is part of the mitochondrial calcium transporter located in the inner membrane and involved in calcium import. Therefore, results indicate a dysregulation in mitochondrial calcium homeostasis with increased calcium import. Mitochondrial dysfunction is a pathological hallmark of PD in the early stage (Yan et al., 2013), and several studies have demonstrated the involvement of pathological αSyn in dysregulated mitochondrial homeostasis, morphology and function (Hsu et al., 2000; Sohrabi et al., 2023). In a previous study, we have shown that H-αSynOs induced mitochondrial morphological abnormalities in the mesencephalon (Boi et al., 2020). Moreover, recent studies have demonstrated that αSyn is pivotal for calcium homeostasis within the HC via the regulation of mitochondrial calcium intake, and loss of the *SNCA* gene results in calcium overload and oxidative stress in the HC associated with spatial memory impairment (Wang et al., 2023).

Among DGEs, members of the potassium voltage-gated channel were highly dysregulated in the HC of parkinsonian rats. Specifically, the potassium voltage-gated (*Kv*) channel modifier subfamily V was over-expressed, while the *KCNA* gene was downregulated in the HC of H-

αSynOs-infused rats. Of note, the PPI analysis displayed the highest node degree in relation to the *KCNA* gene, encoding for potassium voltage-gated channel A1. The *Kv* channel family in the brain plays essential regulatory roles in both neurons, where it regulates neuronal excitability (Chen et al., 2023; Misonou et al., 2005) and in glia, where the *Kv* contributes to neuroinflammatory responses, being upregulated in pro-inflammatory microglia in response to several stressors (Di Lucente et al., 2018; Otuyemi et al., 2023; Sarkar et al., 2020). In PD models, *Kv* alterations have been investigated in motor-related regions such as the striatum and mesencephalon, and have been suggested to be responsible for irregular striatal neuronal firing as well as to boost apoptosis and neurodegeneration (Baranauskas et al., 1999; Chao et al., 2018). Moreover, both in PD models and postmortem human PD brain, *Kv* was upregulated in the mesencephalon by aggregated αSyn (Sarkar et al., 2020). Although little is known on *Kv* alteration in cognition related regions in PD, hippocampal *Kv* channels play a role in the altered neuronal excitability underlying Alzheimer's disease pathology and memory impairment (Piccialli et al., 2022). Interestingly, by using the database Gene Set Enrichment Analysis (GSEA) we found overlapping DEGs between our PD model and studies in PD patients. Among these genes, our study showed that the *SLC7A5* gene was differentially expressed, and the same gene was listed among DEGs in the PD brain (Cappelletti et al., 2023). *SLC7A5* is a membrane transporter that was recently found altered in a mouse model of Alzheimer's disease, likely reflecting vascular alterations, but was never investigated in PD models (Puris et al., 2023).

Furthermore, the PPI analysis revealed the highest node degree for VIM (vimentin) and CRYAB (αB-crystallin), both cytoskeleton proteins which play critical roles in cytoskeletal transport and pathological aggregation/remodelling of neurofilaments, key aspects of PD pathology (Lowe et al., 1992; Novak et al., 2022). We found that *VIM* was down-regulated in H-αSynOs-treated samples. Of note, a reduced amount of vimentin in skin fibroblasts and *VIM* expression in iPSC from patients carrying parkin mutations have been previously reported and related with the PD pathology (Novak et al., 2022; Siciliano et al., 2020).

5. Conclusions

MCI is a common trait often associated with early motor disorder in PD, whose neuropathological substrate is yet poorly understood. We presented a study largely informative on genes whose expression is altered in cognition-related brain regions in a preclinical PD model featuring the early motor PD stage with MCI. The investigation of DEGs in ACC and HC revealed changes highly region-specific, showing that gene patterns were referable to different functional clusters. While innate and adaptive immune responses were mostly dysregulated in the ACC, genes involved in mitochondrial homeostasis and generally neuronal function were mostly affected in the HC. We suggest that soluble αSynOs undergo pathological seeding and spreading through the connectome, reaching areas distant from the infusion site, where they elicit region specific changes in gene expression. Results provide novel insights for the understanding of MCI neuropathology in PD.

CRediT authorship contribution statement

Maria Francesca Manchinu: Conceptualization, Investigation, Methodology, Project administration, Resources, Supervision, Validation, Writing – original draft. **Mauro Pala:** Data curation, Formal analysis, Investigation, Methodology, Software, Validation, Visualization, Writing – original draft. **Maria Francesca Palmas:** Formal analysis, Methodology, Validation, Visualization, Writing – original draft. **Maria Antonietta Diana:** Methodology. **Andrea Maschio:** Investigation, Methodology, Software. **Michela Etzi:** Formal analysis, Methodology. **Augusta Pisanu:** Methodology. **Francesca Isabella Diana:** Data curation, Methodology. **Jacopo Marongiu:** Formal analysis, Methodology. **Silvia Mansueto:** Methodology. **Ezio Carboni:** Conceptualization, Supervision, Writing – review & editing. **Giuliana Fusco:** Investigation, Methodology. **Alfonso De Simone:** Conceptualization, Data curation, Writing – review & editing. **Anna R. Carta:** Conceptualization, Funding acquisition, Supervision, Writing – review & editing.

Declaration of Competing Interest

None.

Data availability

Data will be made available on request.

Acknowledgements

This work was co-funded by Fondazione di Sardegna Grant numbers: F75F21001250007.

Appendix A. Supplementary data

Supplementary data to this article can be found online at https://doi.org/10.1016/j.expneurol.2023.114651.

References

Aarsland, D., Creese, B., Politis, M., Chaudhuri, K.R., Ffytche, D.H., Weintraub, D., Ballard, C., 2017. Cognitive decline in Parkinson disease. Nat. Rev. Neurol. 13, 217–231. https://doi.org/10.1038/nrneurol.2017.27.

Aarsland, D., Batzu, L., Halliday, G.M., Geurtsen, G.J., Ballard, C., Ray Chaudhuri, K., Weintraub, D., 2021. Parkinson disease-associated cognitive impairment. Nat. Rev. Dis. Prim. 7, 47. https://doi.org/10.1038/s41572-021-00280-3.

Anders, S., Pyl, P.T., Huber, W., 2015. HTSeq–a Python framework to work with high-throughput sequencing data. Bioinformatics 31, 166–169. https://doi.org/10.1093/bioinformatics/btu638.

Andrews, S., 2010. FastQC: A quality control tool for high throughput sequence data. Available online at. http://www.bioinformatics.babraham.ac.uk/projects/fastqc [WWW Document].

Baranauskas, G., Tkatch, T., Surmeier, D.J., 1999. Delayed rectifier currents in rat globus pallidus neurons are attributable to Kv2.1 and Kv3.1/3.2 K(+) channels. J. Neurosci. 19, 6394–6404. https://doi.org/10.1523/JNEUROSCI.19-15-06394.1999.

Benoit, S.M., Xu, H., Schmid, S., Alexandrova, R., Kaur, G., Thiruvahindrapuram, B., Pereira, S.L., Jog, M., Hebb, M.O., 2020. Expanding the search for genetic biomarkers of Parkinson's disease into the living brain. Neurobiol. Dis. 140, 104872 https://doi.org/10.1016/j.nbd.2020.104872.

Boi, L., Pisanu, A., Palmas, M.F., Fusco, G., Carboni, E., Casu, M.A., Satta, V., Scherma, M., Janda, E., Mocci, I., Mulas, G., Ena, A., Spiga, S., Fadda, P., De Simone, A., Carta, A.R., 2020. Modeling Parkinson's disease neuropathology and symptoms by intranigral inoculation of preformed human α-synuclein oligomers. Int. J. Mol. Sci. 21 https://doi.org/10.3390/ijms21228535.

Braak, H., Rüb, U., Jansen Steur, E.N.H., Del Tredici, K., de Vos, R.A.I., 2005. Cognitive status correlates with neuropathologic stage in Parkinson disease. Neurology 64, 1404–1410. https://doi.org/10.1212/01.WNL.0000158422.41380.82.

Brochard, V., Combadière, B., Prigent, A., Laouar, Y., Perrin, A., Beray-Berthat, V., Bonduelle, O., Alvarez-Fischer, D., Callebert, J., Launay, J.-M., Duyckaerts, C., Flavell, R.A., Hirsch, E.C., Hunot, S., 2009. Infiltration of CD4+ lymphocytes into the brain contributes to neurodegeneration in a mouse model of Parkinson disease. J. Clin. Invest. 119, 182–192. https://doi.org/10.1172/JCI36470.

Cao, S., Standaert, D.G., Harms, A.S., 2012. The gamma chain subunit of Fc receptors is required for alpha-synuclein-induced pro-inflammatory signaling in microglia. J. Neuroinflammation 9, 259. https://doi.org/10.1186/1742-2094-9-259.

Cappelletti, C., Henriksen, S.P., Geut, H., Rozemuller, A.J.M., van de Berg, W.D.J., Pihlstrøm, L., Toft, M., 2023. Transcriptomic profiling of Parkinson's disease brains reveals disease stage specific gene expression changes. Acta Neuropathol. 146, 227–244. https://doi.org/10.1007/s00401-023-02597-7.

Carta, A.R., Boi, L., Pisanu, A., Palmas, M.F., Carboni, E., De Simone, A., 2020. Advances in modelling alpha-synuclein-induced Parkinson's diseases in rodents: virus-based models versus inoculation of exogenous preformed toxic species. J. Neurosci. Methods 338, 108685. https://doi.org/10.1016/j.jneumeth.2020.108685.

Chao, R.-Y., Cheng, C.-H., Wu, S.-N., Chen, P.-C., 2018. Defective trafficking of Kv2.1 channels in MPTP-induced nigrostriatal degeneration. J. Neurochem. 144, 483–497. https://doi.org/10.1111/jnc.14282.

Chen, X., Feng, Y., Quinn, R.J., Pountney, D.L., Richardson, D.R., Mellick, G.D., Ma, L., 2023. Potassium channels in Parkinson's disease: potential roles in its pathogenesis and innovative molecular targets for treatment. Pharmacol. Rev. 75, 758–788. https://doi.org/10.1124/pharmrev.122.000743.

Chi, L.-M., Wang, L.-P., Jiao, D., 2019. Identification of differentially expressed genes and long noncoding RNAs associated with Parkinson's disease. Parkinsons. Dis. 2019, 6078251. https://doi.org/10.1155/2019/6078251.
Christopher, L., Duff-Canning, S., Koshimori, Y., Segura, B., Boileau, I., Chen, R., Lang, A. E., Houle, S., Rusjan, P., Strafella, A.P., 2015. Salience network and parahippocampal dopamine dysfunction in memory-impaired Parkinson disease. Ann. Neurol. 77, 269–280. https://doi.org/10.1002/ana.24323.
Collins, L.M., Williams-Gray, C.H., 2016. The genetic basis of cognitive impairment and dementia in Parkinson's disease. Front. Psychol. 7, 89. https://doi.org/10.3389/fpsyt.2016.00089.
Dani, A., Chaudhry, A., Mukherjee, P., Rajagopal, D., Bhatia, S., George, A., Bal, V., Rath, S., Mayor, S., 2004. The pathway for MHCII-mediated presentation of endogenous proteins involves peptide transport to the endo-lysosomal compartment. J. Cell Sci. 117, 4219–4230. https://doi.org/10.1242/jcs.01288.
Dauer, W., Przedborski, S., 2003. Parkinson's disease: mechanisms and models. Neuron 39, 889–909. https://doi.org/10.1016/s0896-6273(03)00568-3.
Di Lucente, J., Nguyen, H.M., Wulff, H., Jin, L.-W., Maezawa, I., 2018. The voltage-gated potassium channel Kv1.3 is required for microglial pro-inflammatory activation in vivo. Glia 66, 1881–1895. https://doi.org/10.1002/glia.23457.
Dijkstra, A.A., Ingrassia, A., de Menezes, R.X., van Kesteren, R.E., Rozemuller, A.J.M., Heutink, P., van de Berg, W.D.J., 2015. Evidence for immune response, axonal dysfunction and reduced endocytosis in the substantia Nigra in early stage Parkinson's disease. PLoS One 10, e0128651. https://doi.org/10.1371/journal.pone.0128651.
Diniz, L.P., Araujo, A.P.B., Matias, I., Garcia, M.N., Barros-Aragão, F.G.Q., de Melo Reis, R.A., Foguel, D., Braga, C., Figueiredo, C.P., Romão, L., Gomes, F.C.A., 2020. Astrocyte glutamate transporters are increased in an early sporadic model of synucleinopathy. Neurochem. Int. 138, 104758 https://doi.org/10.1016/j.neuint.2020.104758.
Dobin, A., Davis, C.A., Schlesinger, F., Drenkow, J., Zaleski, C., Jha, S., Batut, P., Chaisson, M., Gingeras, T.R., 2013. STAR: ultrafast universal RNA-seq aligner. Bioinformatics 29, 15–21. https://doi.org/10.1093/bioinformatics/bts635.
Doorn, K.J., Moors, T., Drukarch, B., van de Berg, W.D., Lucassen, P.J., van Dam, A.-M., 2014. Microglial phenotypes and toll-like receptor 2 in the substantia nigra and hippocampus of incidental Lewy body disease cases and Parkinson's disease patients. Acta Neuropathol. Commun. 2, 90. https://doi.org/10.1186/s40478-014-0090-1.
Durrenberger, P.F., Fernando, F.S., Kashefi, S.N., Bonnert, T.P., Seilhean, D., Nait-Oumesmar, B., Schmitt, A., Gebicke-Haerter, P.J., Falkai, P., Grünblatt, E., Palkovits, M., Arzberger, T., Kretzschmar, H., Dexter, D.T., Reynolds, R., 2015. Common mechanisms in neurodegeneration and neuroinflammation: a BrainNet Europe gene expression microarray study. J. Neural Transm. 122, 1055–1068. https://doi.org/10.1007/s00702-014-1293-0.
Edison, P., Ahmed, I., Fan, Z., Hinz, R., Gelosa, G., Ray Chaudhuri, K., Walker, Z., Turkheimer, F.E., Brooks, D.J., 2013. Microglia, amyloid, and glucose metabolism in Parkinson's disease with and without dementia. Neuropsychopharmacol. Off. Publ. Am. Coll. Neuropsychopharmacol. 38, 938–949. https://doi.org/10.1038/npp.2012.255.
Ekman, U., Eriksson, J., Forsgren, L., Mo, S.J., Riklund, K., Nyberg, L., 2012. Functional brain activity and presynaptic dopamine uptake in patients with Parkinson's disease and mild cognitive impairment: a cross-sectional study. Lancet Neurol. 11, 679–687. https://doi.org/10.1016/S1474-4422(12)70138-2.
Fan, Z., Aman, Y., Ahmed, I., Chetelat, G., Landeau, B., Ray Chaudhuri, K., Brooks, D.J., Edison, P., 2015. Influence of microglial activation on neuronal function in Alzheimer's and Parkinson's disease dementia. Alzheimers Dement. 11, 608–621 e7. https://doi.org/10.1016/j.jalz.2014.06.016.
Ferreira, D.G., Temido-Ferreira, M., Vicente Miranda, H., Batalha, V.L., Coelho, J.E., Szegö, É.M., Marques-Morgado, I., Vaz, S.H., Rhee, J.S., Schmitz, M., Zerr, I., Lopes, L.V., Outeiro, T.F., 2017. α-synuclein interacts with PrP(C) to induce cognitive impairment through mGluR5 and NMDAR2B. Nat. Neurosci. 20, 1569–1579. https://doi.org/10.1038/nn.4648.
Fusco, G., Chen, S.W., Williamson, P.T.F., Cascella, R., Perni, M., Jarvis, J.A., Cecchi, C., Vendruscolo, M., Chiti, F., Cremades, N., Ying, L., Dobson, C.M., De Simone, A., 2017. Structural basis of membrane disruption and cellular toxicity by α-synuclein oligomers. Science 358, 1440–1443. https://doi.org/10.1126/science.aan6160.
García-Sanz, P., Orgaz, L., Bueno-Gil, G., Espadas, I., Rodríguez-Traver, E., Kulisevsky, J., Gutierrez, A., Dávila, J.C., González-Polo, R.A., Fuentes, J.M., Mir, P., Vicario, C., Moratalla, R., 2017. N370S-GBA1 mutation causes lysosomal cholesterol accumulation in Parkinson's disease. Mov. Disord. 32, 1409–1422. https://doi.org/10.1002/mds.27119.
García-Sanz, P., Orgaz, L., Fuentes, J.M., Vicario, C., Moratalla, R., 2018. Cholesterol and multilamellar bodies: lysosomal dysfunction in GBA-Parkinson disease. Autophagy 14, 717–718. https://doi.org/10.1080/15548627.2018.1427396.
Gatt, A.P., Duncan, O.F., Attems, J., Francis, P.T., Ballard, C.G., Bateman, J.M., 2016. Dementia in Parkinson's disease is associated with enhanced mitochondrial complex I deficiency. Mov. Disord. 31, 352–359. https://doi.org/10.1002/mds.26513.
Gómez-Benito, M., Granado, N., García-Sanz, P., Michel, A., Dumoulin, M., Moratalla, R., 2020. Modeling Parkinson's disease with the alpha-synuclein protein. Front. Pharmacol. 11, 356. https://doi.org/10.3389/fphar.2020.00356.
Harms, A.S., Cao, S., Rowse, A.L., Thome, A.D., Li, X., Mangieri, L.R., Cron, R.Q., Shacka, J.J., Raman, C., Standaert, D.G., 2013. MHCII is required for α-synuclein-induced activation of microglia, CD4 T cell proliferation, and dopaminergic neurodegeneration. J. Neurosci. 33, 9592–9600. https://doi.org/10.1523/JNEUROSCI.5610-12.2013.
Harris, M.A., Clark, J., Ireland, A., Lomax, J., Ashburner, M., Foulger, R., Eilbeck, K., Lewis, S., Marshall, B., Mungall, C., Richter, J., Rubin, G.M., Blake, J.A., Bult, C., Dolan, M., Drabkin, H., Eppig, J.T., Hill, D.P., Ni, L., Ringwald, M., Balakrishnan, R., Cherry, J.M., Christie, K.R., Costanzo, M.C., Dwight, S.S., Engel, S., Fisk, D.G., Hirschman, J.E., Hong, E.L., Nash, R.S., Sethuraman, A., Theesfeld, C.L., Botstein, D., Dolinski, K., Feierbach, B., Berardini, T., Mundodi, S., Rhee, S.Y., Apweiler, R., Barrell, D., Camon, E., Dimmer, E., Lee, V., Chisholm, R., Gaudet, P., Kibbe, W., Kishore, R., Schwarz, E.M., Sternberg, P., Gwinn, M., Hannick, L., Wortman, J., Berriman, M., Wood, V., de la Cruz, N., Tonellato, P., Jaiswal, P., Seigfried, T., White, R., 2004. The gene ontology (GO) database and informatics resource. Nucleic Acids Res. 32, D258–D261. https://doi.org/10.1093/nar/gkh036.
Hsu, L.J., Sagara, Y., Arroyo, A., Rockenstein, E., Sisk, A., Mallory, M., Wong, J., Takenouchi, T., Hashimoto, M., Masliah, E., 2000. alpha-synuclein promotes mitochondrial deficit and oxidative stress. Am. J. Pathol. 157, 401–410. https://doi.org/10.1016/s0002-9440(10)64553-1.
Imamura, K., Hishikawa, N., Sawada, M., Nagatsu, T., Yoshida, M., Hashizume, Y., 2003. Distribution of major histocompatibility complex class II-positive microglia and cytokine profile of Parkinson's disease brains. Acta Neuropathol. 106, 518–526. https://doi.org/10.1007/s00401-003-0766-2.
Jung, Y.J., Tweedie, D., Scerba, M.T., Kim, D.S., Palmas, M.F., Pisanu, A., Carta, A.R., Greig, N.H., 2021. Repurposing immunomodulatory imide drugs (IMiDs) in neuropsychiatric and neurodegenerative disorders. Front. Neurosci. 15, 656921 https://doi.org/10.3389/fnins.2021.656921.
Kanehisa, M., Furumichi, M., Tanabe, M., Sato, Y., Morishima, K., 2017. KEGG: new perspectives on genomes, pathways, diseases and drugs. Nucleic Acids Res. 45, D353–D361. https://doi.org/10.1093/nar/gkw1092.
Koeglsperger, T., Li, S., Brenneis, C., Saulnier, J.L., Mayo, L., Carrier, Y., Selkoe, D.J., Weiner, H.L., 2013. Impaired glutamate recycling and GluN2B-mediated neuronal calcium overload in mice lacking TGF-β1 in the CNS. Glia 61, 985–1002. https://doi.org/10.1002/glia.22490.
Kouli, A., Camacho, M., Allinson, K., Williams-Gray, C.H., 2020. Neuroinflammation and protein pathology in Parkinson's disease dementia. Acta Neuropathol. Commun. 8, 211. https://doi.org/10.1186/s40478-020-01083-5.
Kövari, E., Gold, G., Herrmann, F.R., Canuto, A., Hof, P.R., Bouras, C., Giannakopoulos, P., 2003. Lewy body densities in the entorhinal and anterior cingulate cortex predict cognitive deficits in Parkinson's disease. Acta Neuropathol. 106, 83–88. https://doi.org/10.1007/s00401-003-0705-2.
Lecca, D., Janda, E., Mulas, G., Diana, A., Martino, C., Angius, F., Spolitu, S., Casu, M.A., Simbula, G., Boi, L., Batetta, B., Spiga, S., Carta, A.R., 2018. Boosting phagocytosis and anti-inflammatory phenotype in microglia mediates neuroprotection by PPARγ agonist MDG548 in Parkinson's disease models. Br. J. Pharmacol. 175, 3298–3314. https://doi.org/10.1111/bph.14214.
Leek, J.T., 2014. svaseq: removing batch effects and other unwanted noise from sequencing data. Nucleic Acids Res. 42, e161 https://doi.org/10.1093/nar/gku864.
Li, J., Sun, Y., Chen, J., 2019. Transcriptome sequencing in a 6-hydroxydopamine rat model of Parkinson's disease. Genes Genet. Syst. 94, 61–69. https://doi.org/10.1266/ggs.18-00036.
Lindestam Arlehamn, C.S., Dhanwani, R., Pham, J., Kuan, R., Frazier, A., Rezende Dutra, J., Phillips, E., Mallal, S., Roederer, M., Marder, K.S., Amara, A.W., Standaert, D.G., Goldman, J.G., Litvan, I., Peters, B., Sulzer, D., Sette, A., 2020. α-Synuclein-specific T cell reactivity is associated with preclinical and early Parkinson's disease. Nat. Commun. 11, 1875. https://doi.org/10.1038/s41467-020-15626-w.
Love, M.I., Huber, W., Anders, S., 2014. Moderated estimation of fold change and dispersion for RNA-seq data with DESeq2. Genome Biol. 15, 550. https://doi.org/10.1186/s13059-014-0550-8.
Lowe, J., Errington, D.R., Lennox, G., Pike, I., Spendlove, I., Landon, M., Mayer, R.J., 1992. Ballooned neurons in several neurodegenerative diseases and stroke contain alpha B crystallin. Neuropathol. Appl. Neurobiol. 18, 341–350. https://doi.org/10.1111/j.1365-2990.1992.tb00796.x.
Luk, K.C., Kehm, V., Carroll, J., Zhang, B., O'Brien, P., Trojanowski, J.Q., Lee, V.M.-Y., 2012. Pathological α-synuclein transmission initiates Parkinson-like neurodegeneration in nontransgenic mice. Science 338, 949–953. https://doi.org/10.1126/science.1227157.
Lyu, Y., Huang, Y., Shi, G., Lei, X., Li, K., Zhou, R., Bai, L., Qin, C., 2021. Transcriptome profiling of five brain regions in a 6-hydroxydopamine rat model of Parkinson's disease. CNS Neurosci. Ther. 27, 1289–1299. https://doi.org/10.1111/cns.13702.
Massagué, J., Wotton, D., 2000. Transcriptional control by the TGF-beta/Smad signaling system. EMBO J. 19, 1745–1754. https://doi.org/10.1093/emboj/19.8.1745.
Matias, I., Diniz, L.P., Araujo, A.P.B., Damico, I.V., de Moura, P., Cabral-Miranda, F., Diniz, F., Parmeggiani, B., de Mello Coelho, V., Leite, R.E.P., Suemoto, C.K., Ferreira, G.C., Kubrusly, R.C.C., Gomes, F.C.A., 2023. Age-associated upregulation of glutamate transporters and glutamine synthetase in senescent astrocytes in vitro and in the mouse and human hippocampus. ASN Neuro 15. https://doi.org/10.1177/17590914231157974, 17590914231157974.
Mattila, P.M., Rinne, J.O., Helenius, H., Dickson, D.W., Röyttä, M., 2000. Alpha-synuclein-immunoreactive cortical Lewy bodies are associated with cognitive impairment in Parkinson's disease. Acta Neuropathol. 100, 285–290. https://doi.org/10.1007/s004019900168.
Misonou, H., Mohapatra, D.P., Trimmer, J.S., 2005. Kv2.1: a voltage-gated k+ channel critical to dynamic control of neuronal excitability. Neurotoxicology 26, 743–752. https://doi.org/10.1016/j.neuro.2005.02.003.
Muslimovic, D., Post, B., Speelman, J.D., Schmand, B., 2005. Cognitive profile of patients with newly diagnosed Parkinson disease. Neurology 65, 1239–1245. https://doi.org/10.1212/01.wnl.0000180516.69442.95.
Novak, G., Kyriakis, D., Grzyb, K., Bernini, M., Rodius, S., Dittmar, G., Finkbeiner, S., Skupin, A., 2022. Single-cell transcriptomics of human iPSC differentiation dynamics reveal a core molecular network of Parkinson's disease. Commun. Biol. 5, 49. https://doi.org/10.1038/s42003-021-02973-7.

Osaki, Y., Morita, Y., Fukumoto, M., Akagi, N., Yoshida, S., Doi, Y., 2009. Cross-sectional and longitudinal studies of three-dimensional stereotactic surface projection SPECT analysis in Parkinson's disease. Mov. Disord. 24, 1475–1480. https://doi.org/10.1002/mds.22623.

Otuyemi, B., Jackson, T., Ma, R., Monteiro, A.R., Seifi, M., Swinny, J.D., 2023. Domain and cell type-specific immunolocalisation of voltage-gated potassium channels in the mouse striatum. J. Chem. Neuroanat. 128, 102233 https://doi.org/10.1016/j.jchemneu.2023.102233.

Palmas, M.F., Ena, A., Burgaletto, C., Casu, M.A., Cantarella, G., Carboni, E., Etzi, M., De Simone, A., Fusco, G., Cardia, M.C., Lai, F., Picci, L., Tweedie, D., Scerba, M.T., Coroneo, V., Bernardini, R., Greig, N.H., Pisanu, A., Carta, A.R., 2022a. Repurposing Pomalidomide as a neuroprotective drug: efficacy in an alpha-synuclein-based model of Parkinson's disease. Neurother. J. Am. Soc. Exp. Neurother. 19, 305–324. https://doi.org/10.1007/s13311-022-01182-2.

Palmas, M.F., Etzi, M., Pisanu, A., Camoglio, C., Sagheddu, C., Santoni, M., Manchinu, M. F., Pala, M., Fusco, G., De Simone, A., Picci, L., Mulas, G., Spiga, S., Scherma, M., Fadda, P., Pistis, M., Simola, N., Carboni, E., Carta, A.R., 2022b. The intranigral infusion of human-alpha synuclein oligomers induces a cognitive impairment in rats associated with changes in neuronal firing and neuroinflammation in the anterior cingulate cortex. Cells 11. https://doi.org/10.3390/cells11172628.

Paxinos, G., Watson, C., 2006. The rat brain in stereotaxic coordinates: hard cover edition. Elsevier.

Piccialli, I., Sisalli, M.J., de Rosa, V., Boscia, F., Tedeschi, V., Secondo, A., Pannaccione, A., 2022. Increased K(V)2.1 channel clustering underlies the reduction of delayed rectifier K(+) currents in hippocampal neurons of the Tg2576 Alzheimer's disease mouse. Cells 11. https://doi.org/10.3390/cells11182820.

Pisanu, A., Lecca, D., Mulas, G., Wardas, J., Simbula, G., Spiga, S., Carta, A.R., 2014. Dynamic changes in pro- and anti-inflammatory cytokines in microglia after PPAR-γ agonist neuroprotective treatment in the MPTPp mouse model of progressive Parkinson's disease. Neurobiol. Dis. 71, 280–291. https://doi.org/10.1016/j.nbd.2014.08.011.

Puris, E., Saveleva, L., de Sousa Maciel, I., Kanninen, K.M., Auriola, S., Fricker, G., 2023. Protein expression of amino acid transporters is altered in isolated cerebral microvessels of 5xFAD mouse model of Alzheimer's disease. Mol. Neurobiol. 60, 732–748. https://doi.org/10.1007/s12035-022-03111-y.

Quan, W., Li, J., Jin, X., Liu, L., Zhang, Q., Qin, Y., Pei, X., Chen, J., 2021. Identification of potential core genes in Parkinson's disease using bioinformatics analysis. Parkinsons. Dis. 2021, 1690341. https://doi.org/10.1155/2021/1690341.

Raudvere, U., Kolberg, L., Kuzmin, I., Arak, T., Adler, P., Peterson, H., Vilo, J., 2019. g: profiler: a web server for functional enrichment analysis and conversions of gene lists (2019 update). Nucleic Acids Res. 47, W191–W198. https://doi.org/10.1093/nar/gkz369.

Rostami, J., Fotaki, G., Sirois, J., Mzezewa, R., Bergström, J., Essand, M., Healy, L., Erlandsson, A., 2020. Astrocytes have the capacity to act as antigen-presenting cells in the Parkinson's disease brain. J. Neuroinflammation 17, 119. https://doi.org/10.1186/s12974-020-01776-7.

Sarkar, S., Nguyen, H.M., Malovic, E., Luo, J., Langley, M., Palanisamy, B.N., Singh, N., Manne, S., Neal, M., Gabrielle, M., Abdalla, A., Anantharam, P., Rokad, D., Panicker, N., Singh, V., Ay, M., Charli, A., Harischandra, D., Jin, L.-W., Jin, H., Rangaraju, S., Anantharam, V., Wulff, H., Kanthasamy, A.G., 2020. Kv1.3 modulates neuroinflammation and neurodegeneration in Parkinson's disease. J. Clin. Invest. 130, 4195–4212. https://doi.org/10.1172/JCI136174.

Sauerbier, A., Rosa-Grilo, M., Qamar, M.A., Chaudhuri, K.R., 2017. Nonmotor subtyping in Parkinson's disease. Int. Rev. Neurobiol. 133, 447–478. https://doi.org/10.1016/bs.irn.2017.05.011.

Sawamoto, N., Piccini, P., Hotton, G., Pavese, N., Thielemans, K., Brooks, D.J., 2008. Cognitive deficits and striato-frontal dopamine release in Parkinson's disease. Brain 131, 1294–1302. https://doi.org/10.1093/brain/awn054.

Severiano E Sousa, C., Fabbri, M., Godinho, C., Moiron Simões, R., Chendo, I., Coelho, M., Pavão Martins, I., Ferreira, J.J., 2022. Profile of cognitive impairment in late-stage Parkinson's disease. Brain Behav. 12, e2537 https://doi.org/10.1002/brb3.2537.

Siciliano, R.A., Mazzeo, M.F., Ferretta, A., Pacelli, C., Rosato, A., Papa, F., Scacco, S., Papa, S., Cocco, T., Lippolis, R., 2020. Decreased amount of vimentin N-terminal truncated proteolytic products in parkin-mutant skin fibroblasts. Biochem. Biophys. Res. Commun. 521, 693–698. https://doi.org/10.1016/j.bbrc.2019.10.154.

Sohrabi, T., Mirzaei-Behbahani, B., Zadali, R., Pirhaghi, M., Morozova-Roche, L.A., Meratan, A.A., 2023. Common mechanisms underlying α-synuclein-induced mitochondrial dysfunction in Parkinson's disease. J. Mol. Biol. 435, 167992 https://doi.org/10.1016/j.jmb.2023.167992.

Sorrentino, Z.A., Brooks, M.M.T., Hudson 3rd, V., Rutherford, N.J., Golde, T.E., Giasson, B.I., Chakrabarty, P., 2017. Intrastriatal injection of α-synuclein can lead to widespread synucleinopathy independent of neuroanatomic connectivity. Mol. Neurodegener. 12, 40. https://doi.org/10.1186/s13024-017-0182-z.

Strimmer, K., 2008. Fdrtool: a versatile R package for estimating local and tail area-based false discovery rates. Bioinformatics 24, 1461–1462. https://doi.org/10.1093/bioinformatics/btn209.

Sulzer, D., Alcalay, R.N., Garretti, F., Cote, L., Kanter, E., Agin-Liebes, J., Liong, C., McMurtrey, C., Hildebrand, W.H., Mao, X., Dawson, V.L., Dawson, T.M., Oseroff, C., Pham, J., Sidney, J., Dillon, M.B., Carpenter, C., Weiskopf, D., Phillips, E., Mallal, S., Peters, B., Frazier, A., Lindestam Arlehamn, C.S., Sette, A., 2017. T cells from patients with Parkinson's disease recognize α-synuclein peptides. Nature 546, 656–661. https://doi.org/10.1038/nature22815.

Szklarczyk, D., Franceschini, A., Wyder, S., Forslund, K., Heller, D., Huerta-Cepas, J., Simonovic, M., Roth, A., Santos, A., Tsafou, K.P., Kuhn, M., Bork, P., Jensen, L.J., von Mering, C., 2015. STRING v10: protein-protein interaction networks, integrated over the tree of life. Nucleic Acids Res. 43, D447–D452. https://doi.org/10.1093/nar/gku1003.

Todd, A.C., Hardingham, G.E., 2020. The regulation of astrocytic glutamate transporters in health and neurodegenerative diseases. Int. J. Mol. Sci. 21 https://doi.org/10.3390/ijms21249607.

Wang, Y., Miao, Z., Xu, C., Cai, Y., Yang, Y., Hu, Y., Zhao, M., Shao, Y., Li, Z., Chen, J., Chen, S., Wang, L., 2023. Pathological convergence of APP and SNCA deficiency in hippocampal degeneration of young rats. Cell Death Dis. 14, 325. https://doi.org/10.1038/s41419-023-05846-5.

Williams-Gray, C.H., Evans, J.R., Goris, A., Foltynie, T., Ban, M., Robbins, T.W., Brayne, C., Kolachana, B.S., Weinberger, D.R., Sawcer, S.J., Barker, R.A., 2009. The distinct cognitive syndromes of Parkinson's disease: 5 year follow-up of the CamPaIGN cohort. Brain 132, 2958–2969. https://doi.org/10.1093/brain/awp245.

Williams-Gray, C.H., Wijeyekoon, R., Yarnall, A.J., Lawson, R.A., Breen, D.P., Evans, J. R., Cummins, G.A., Duncan, G.W., Khoo, T.K., Burn, D.J., Barker, R.A., 2016. Serum immune markers and disease progression in an incident Parkinson's disease cohort (ICICLE-PD). Mov. Disord. 31, 995–1003. https://doi.org/10.1002/mds.26563.

Wilson, H., Dervenoulas, G., Pagano, G., Tyacke, R.J., Polychronis, S., Myers, J., Gunn, R. N., Rabiner, E.A., Nutt, D., Politis, M., 2019. Imidazoline 2 binding sites reflecting astroglia pathology in Parkinson's disease: an in vivo11C-BU99008 PET study. Brain 142, 3116–3128. https://doi.org/10.1093/brain/awz260.

Xie, S., Yang, J., Huang, S., Fan, Y., Xu, T., He, J., Guo, J., Ji, X., Wang, Z., Li, P., Chen, J., Zhang, Y., 2022. Disrupted myelination network in the cingulate cortex of Parkinson's disease. IET Syst. Biol. 16, 98–119. https://doi.org/10.1049/syb2.12043.

Yan, M.H., Wang, X., Zhu, X., 2013. Mitochondrial defects and oxidative stress in Alzheimer disease and Parkinson disease. Free Radic. Biol. Med. 62, 90–101. https://doi.org/10.1016/j.freeradbiomed.2012.11.014.